J. Fluid Mech. (1982), *vol.* 120, *pp.* 123–138
Printed in Great Britain

Nonlinear Marangoni convection in bounded layers. Part 2. Rectangular cylindrical containers

By S. ROSENBLAT, G. M. HOMSY AND S. H. DAVIS
SHD Associates, Inc., 2735 Simpson St, Evanston, IL 60201, U.S.A.

(Received 16 June 1981 and in revised form 14 December 1981)

Attention is confined to roll-cell development and roll-cell interaction appropriate to one horizontal dimension larger than either the other horizontal dimension or the depth. At simple eigenvalues M_c, the roll-cell amplitude and transport fields can be obtained. Near those aspect ratios corresponding to double eigenvalues M_c, where two roll-cell states of linear theory are equally likely, the nonlinear theory predicts sequences of transitions from one steady convective state to another as the Marangoni number is increased. Direct comparisons are made of the results here with those of the previous paper for Marangoni convection in circular cylinders. Time-periodic convection is possible in certain cases.

1. Introduction

In part 1 of this study (Rosenblat, Davis & Homsy 1982) we discussed Marangoni instabilities in a circular cylinder and distinguished between simple eigenvalues and double eigenvalues, where secondary bifurcations are possible.

In the present paper, we examine Marangoni instability in rectangular containers. As before, we assume that the upper free surface is non-deformable, and the side walls are adiabatic and impermeable but 'slippery', which in the rectangular geometry corresponds to zero shear stress applied on the boundary. We use the asymptotic theory of Rosenblat (1979) to examine the steady convective states near M_c and how transitions from one state to another occur. We limit ourselves to interactions of modes in the form of two-dimensional roll-cells, which are predicted for rectangular containers having the shorter side comparable to the depth and the longer side larger than he depth. Since much of the full development is similar to that in part 1, we give only those details which distinguish convection in a rectangular container from convection in a circular cylinder.

2. Formulation

Consider a viscous liquid, which partially fills a container of rectangular cross-section. The mean depth of the liquid is d and a horizontal cross-section has lengths $a_1 d$ and $a_2 d$ in the x- and y-directions respectively. Hence a_1 and a_2 are the aspect ratios. The axis of the cylinder is antiparallel to the direction of gravity, and the upper surface of the liquid is open to an ambient gas.

The development of the non-dimensional nonlinear disturbance equations and boundary conditions parallels that in part 1. Again, in the limit of small capillary number and when the lateral boundaries are adiabatic and impenetrable but 'slippery', we obtain the following nonlinear problem.

From equations (2.7)–(2.9) of part 1

$$Pr^{-1}M\left\{\frac{\partial \mathbf{v}}{\partial t}+(\mathbf{v}\,.\,\boldsymbol{\nabla})\,\mathbf{v}\right\} = -\nabla p+\nabla^2\mathbf{v}+M^{-1}R\theta\hat{\mathbf{z}}, \tag{2.1}$$

$$\nabla\,.\,\mathbf{v} = 0, \tag{2.2}$$

$$M\left\{\frac{\partial \theta}{\partial t}-w+(\mathbf{v}\,.\,\boldsymbol{\nabla})\,\theta\right\} = \nabla^2\theta, \tag{2.3}$$

where M, R and Pr are the Marangoni, Rayleigh and Prandtl numbers defined in equations (2.16a–c) of part 1.

The bottom of the box is a rigid perfect conductor, so that

$$\theta = 0 \quad (z=0, \quad 0 \leqslant x \leqslant a_1, \quad 0 \leqslant y \leqslant a_2), \tag{2.4a}$$

$$\mathbf{v} = \mathbf{0} \quad (z=0, \quad 0 \leqslant x \leqslant a_1, \quad 0 \leqslant y \leqslant a_2). \tag{2.4b}$$

Since the capillary number is zero, the upper surface is flat, so that the heat-transfer condition is

$$\frac{\partial \theta}{\partial z}+L\theta = 0 \quad (z=1, \quad 0 \leqslant x \leqslant a_1, \quad 0 \leqslant y \leqslant a_2), \tag{2.5a}$$

and the kinematic condition is

$$w = 0 \quad (z=1, \quad 0 \leqslant x \leqslant a_1, \quad 0 \leqslant y \leqslant a_2). \tag{2.5b}$$

The conditions of thermocapillarity become

$$u_z+w_x+\theta_x = v_z+w_y+\theta_y = 0 \quad (z=1, \quad 0 \leqslant x \leqslant a_1, \quad 0 \leqslant y \leqslant a_2). \tag{2.5c}$$

Finally, the 'slippery' side walls reduce in Cartesian co-ordinates to adiabatic, impermeable stress-free planes. These conditions take the form

$$u = w_x = v_x = \theta_x = 0 \quad (x = 0, a_1; \quad 0 \leqslant y \leqslant a_2, \quad 0 \leqslant z \leqslant 1), \tag{2.6a}$$

$$v = w_y = u_y = \theta_y = 0 \quad (y = 0, a_2; \quad 0 \leqslant x \leqslant a_1, \quad 0 \leqslant z \leqslant 1). \tag{2.6b}$$

3. Linear stability problem

The critical Marangoni number at which the conduction solution loses stability is determined from linearization of the system (2.1)–(2.3) together with the (linear) boundary conditions (2.4)–(2.6). As in part 1, we assume that M_c occurs at a state of neutral stability, so that the governing linearized equations become

$$\nabla^4 w+M^{-1}R\nabla_1^2\theta = 0, \tag{3.1a}$$

$$\nabla^2\theta+Mw = 0. \tag{3.1b}$$

System (3.1) plus boundary conditions (2.4)–(2.6) may be solved by seeking separable solutions of the form

$$w(x,y,z) = \cos\left[m_1\pi x/a_1\right]\cos\left[m_2\pi y/a_2\right]Y(z), \tag{3.2a}$$

$$\theta(x,y,z) = \cos\left[m_1\pi x/a_1\right]\cos\left[m_2\pi y/a_2\right]X(z), \tag{3.2b}$$

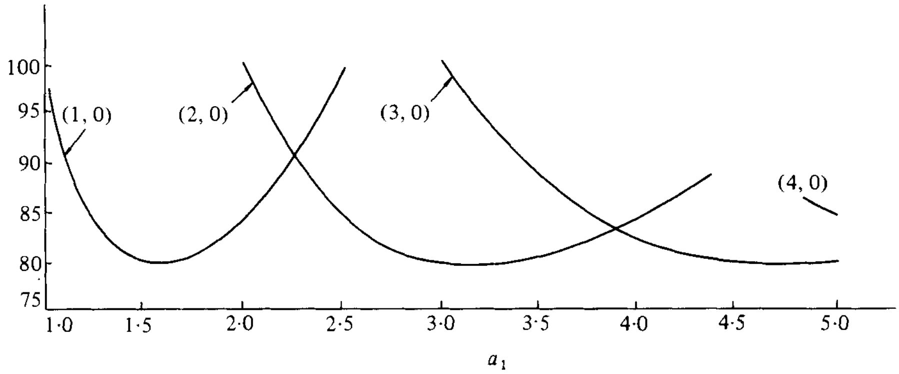

FIGURE 1. Stability curves M versus a_1 for $L = 0$ at $a_2 = 0{\cdot}5$. The pairs (m_1, m_2) denote integral number of cycles in (a_1, a_2).

with similar definitions for u and v. Here X and Y are the same functions as those in part 1. Here m_1 and m_2 run over all non-negative integers.

When forms (3.2) are substituted into (3.1), an effective wavenumber λ appears, where

$$\lambda^2 = [(m_1/a_1)^2 + (m_2/a_2)^2]\,\pi^2. \tag{3.3}$$

The effects of buoyancy through the Rayleigh number R and the effects of the free surface being a poor insulator through the surface Biot number can be explored as in part 1. The effects are the same in that increasing R decreases M_c, and increasing L increases M_c. These results will not be presented here. We shall confine ourselves to $R = 0$ and $L = 0$. In this case we find that

$$M(\lambda) = \frac{8\lambda^2(\lambda - \sinh\lambda\,\cosh\lambda)\cosh\lambda}{\lambda^2\cosh\lambda - \sinh^3\lambda}. \tag{3.4}$$

We note that, for an infinite layer, λ is the overall wavenumber, which takes on all values $[0, \infty)$. $M(\lambda)$ would then have the minimum $M_\infty \simeq 79{\cdot}6$ for $\lambda_\infty \simeq 2$. This result is due to Pearson (1958). For the present enclosed layer, $M(\lambda)$ must be minimized over only those admissible λ given by (3.3).

The relationship between the box aspect ratios and the mode of convection, indicated by the integers (m_1, m_2), is given implicitly by (3.3) and (3.4). We have evaluated this relationship for a range of box sizes for all possible modes of convection. The results are given in figures 1–6, in which M is given as a function of a_1 for fixed values of a_2. For clarity, modes having large critical Marangoni numbers are not shown. Consider first the case of $a_2 = 0{\cdot}5$ shown in figure 1. As the box size a_1 increases, the preferred mode, i.e. the mode having the lowest critical Marangoni number, changes in a specific way. This sequence is among modes for which $m_2 = 0$. Thus we have two-dimensional roll cells whose axes are aligned with the shorter dimension of the box. We shall call these x-rolls. It is seen that for box sizes $a_1 \simeq \frac{1}{2}m_1\pi$, with $m_1 = 1, 2, 3, \ldots$, that $\lambda \simeq 2$ and the critical Marangoni number is a minimum at the value $M_\infty \simeq 79{\cdot}6$ appropriate to infinite layers. Away from these values, the side walls exert a stabilizing influence, even though they are 'slippery'. While the fact that several box sizes can have the same $M = M_\infty$ is presumably an artifact of the use of the slip-wall boundary conditions, the existence and progression of preferred modes due to the finite size of the container is not.

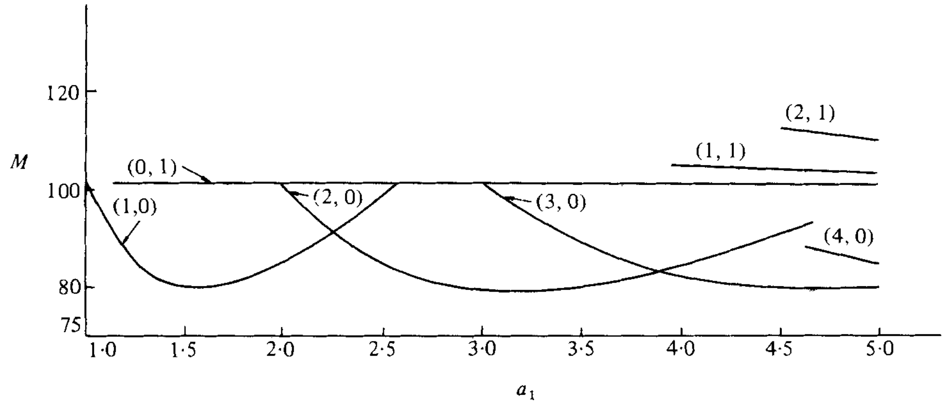

FIGURE 2. Stability curves M versus a_1 for $L = 0$ at $a_2 = 1{\cdot}0$. The pairs (m_1, m_2) denote integral number of cycles in (a_1, a_2).

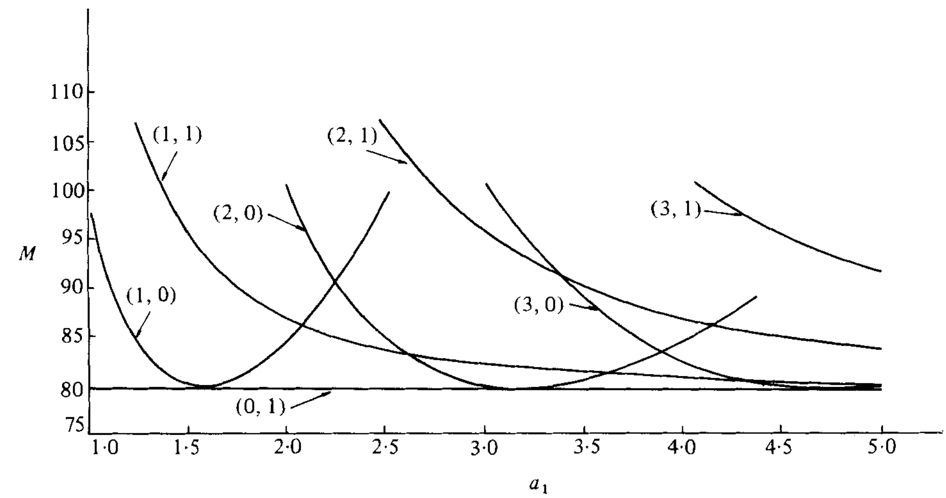

FIGURE 3. Stability curves M versus a_1 for $L = 0$ at $a_2 = 1{\cdot}5$. The pairs (m_1, m_2) denote integral number of cycles in (a_1, a_2).

In the case of buoyancy-driven convection, the dependence of M on box size is monotonic but has kinks at the points of mode switching (Davis 1967), and the effect of side walls is to align the roll axes with the shorter side of the box. This is the same progression and alignment as predicted here for $a_2 = 0{\cdot}5$, but we shall see below that the present treatment leads to some predictions of preferred mode orientation that are presumably artifacts of the slip-wall boundary conditions.

To summarize, the curves in figure 1 predict preferred modes consisting of x-rolls, and the progression is to add more x-rolls as the box size increases. Of particular interest are the aspect ratios at which two modes have the same critical M, this is a double eigenvalue of the linear theory.

Figure 2 shows the results for $a_2 = 1{\cdot}0$. Since the modes with $m_2 = 0$ are unaffected by the length a_2 the lower curves are identical with those of figure 1. We anticipate, however, that, as a_2 approaches $\frac{1}{2}m_2$, there are two-dimensional rolls with axes aligned with the *longer* side of the box (y-rolls), which might have lower critical Marangoni numbers than the x-rolls. This is not yet the case for the $(0, 1)$ mode for the conditions

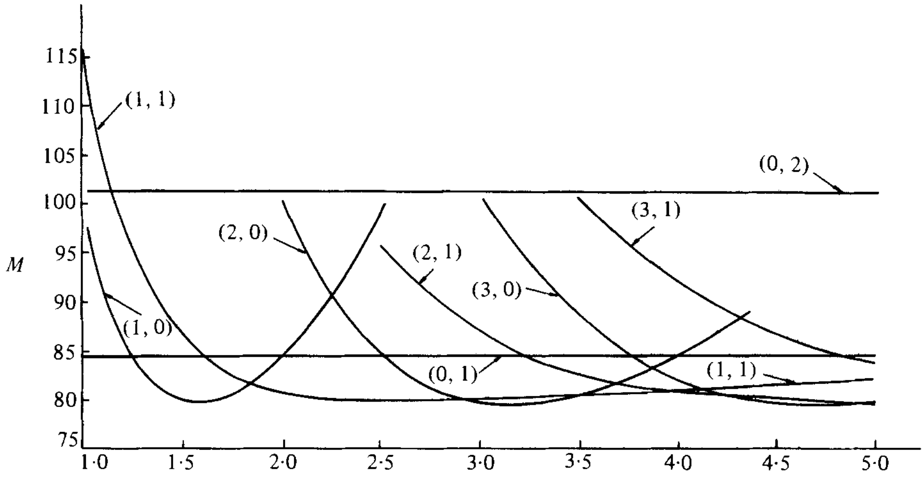

FIGURE 4. Stability curves M versus a_1 for $L = 0$ at $a_2 = 2{\cdot}0$. The pairs (m_1, m_2) denote integral number of cycles in (a_1, a_2).

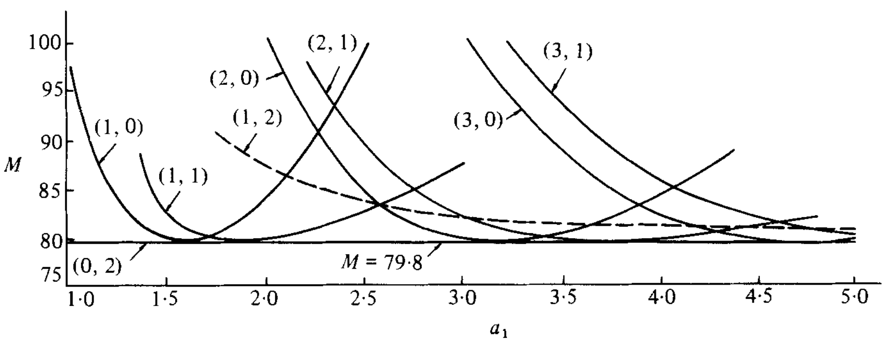

FIGURE 5. Stability curves M versus a_1 for $L = 0$ at $a_2 = 3{\cdot}0$. The pairs (m_1, m_2) denote integral number of cycles in (a_1, a_2).

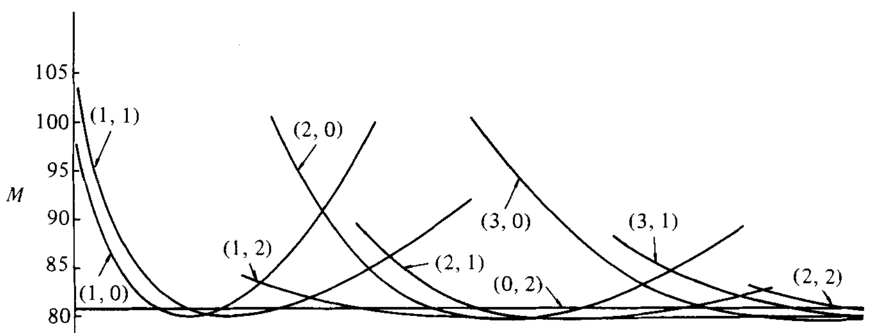

FIGURE 6. Stability curves M versus a_1 for $L = 0$ at $a_2 = 3{\cdot}5$. The pairs (m_1, m_2) denote integral number of cycles in (a_1, a_2).

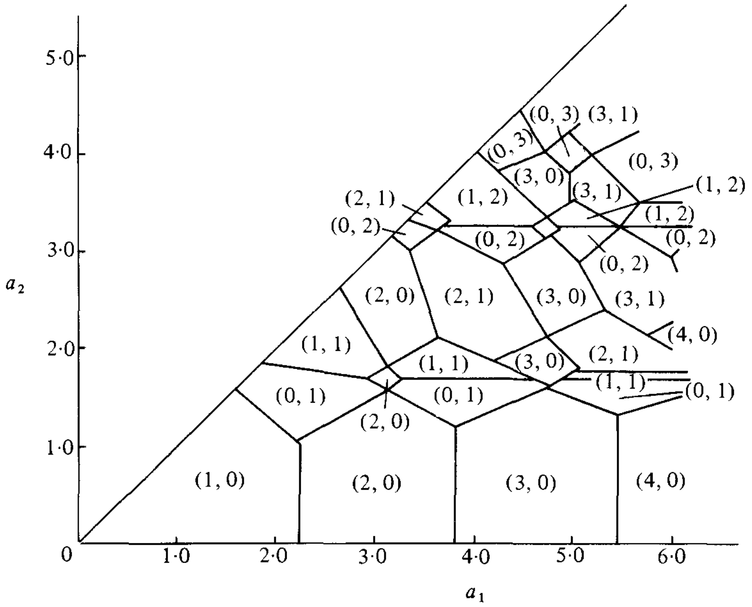

FIGURE 7. Stability map for preferred mode as a function of a_1 and a_2. $L = 0$. The figure is symmetric about $a_1 = a_2$. The pairs (m_1, m_2) denote integral number of cycles in (a_1, a_2).

of figure 2, but becomes so for the conditions of figure 3. Finally, we note the occurrence of more complex three-dimensional modes of convection, e.g. the (1, 1) and (2, 1) modes, having Marangoni numbers close to, but above, those for x-rolls.

Figure 3 gives results for $a_2 = 1\cdot5$, and shows several complex features. First we note that the (0, 1) y-roll has $M \simeq M_\infty$ for this value of a_2, independent of a_1, and hence is often the preferred mode. However, since $a_2 \neq \frac{1}{2}\pi$, there are small ranges of box sizes located near $a_1 = \frac{1}{2}\pi m_1$ for which x-rolls are preferred. We also note that three-dimensional modes, e.g. the (1, 1) and (2, 1), become closer to being preferred. At $a_2 = 2\cdot0$ the results shown in figure 4 indicate that the y-rolls (0, 1), (0, 2) are no longer preferred, and the three-dimensional (1, 1) and (2, 1) modes are preferred over x-rolls for some range of values of a_1 away from $a_1 = \frac{1}{2}m_1\pi$. For $a_2 = 3\cdot0$ (i.e. close to π) figure 5 shows that a situation analogous to that in figure 3 occurs; the y-roll (0, 2) has $M \simeq M_\infty$, and is preferred for all box sizes a_1 away from $\frac{1}{2}m_1\pi$. Finally, as shown in figure 6, as a_2 increases, the number of modes competing and having $M \simeq M_\infty$ increases, and the envelope of these neutral curves becomes nearly the horizontal line $M = M_\infty$. This reflects the diminished effect of the side walls in determining the preferred mode.

The results may be summarized by a map in the (a_1, a_2)-plane of the preferred modes. We note that the pattern of preferred modes must be antisymmetric about $a_1 = a_2$, corresponding to a rotation of the co-ordinate system. Thus $M(a_1, a_2) = M(a_2, a_1)$, and the preferred modes, $(m_1(a_1, a_2), m_2(a_1, a_2)) = (m_2(a_2, a_1), m_1(a_2, a_1))$. It is clear from the previous discussion that this map will be complex, and that, as a_1 and a_2 become large, many modes will have values of the critical Marangoni number close to that for the preferred modes. This map is shown in figure 7. With one exception, it is difficult to speculate on the degree to which this complexity depends upon the use of slip-wall boundary conditions. Complexity of this degree does not occur for buoyancy-driven convection in a box (Davis 1967), but does occur for buoyancy-driven convection in a bounded porous medium (Beck 1972). The persistence of y-rolls and x-rolls at $a_1 \simeq \frac{1}{2}m_1\pi, a_2 \simeq \frac{1}{2}m_2\pi$ ($m_1, m_2 = 0, 1, 2, \ldots$) respectively, will not occur if more realistic no-slip boundary conditions are applied. Careful study of results similar to those in figures 1–6 indicates that much of the complex mode-switching is due to the neutral curve for y-rolls (x-rolls), being a horizontal line, intersecting many times the neutral curve for other modes. No-slip side-wall conditions do not admit pure x-rolls or y-rolls, with the result that the neutral curves for modes that are close to y-rolls, (x-rolls), may not exhibit as many intersections. However, this does not imply that the bifurcation theory developed below will be necessarily simpler, as these modes may continue to be near-multiple eigenvalues of the linear theory.

4. Eigenfunction expansions

In the nonlinear theory we focus on certain special interactions appropriate to one horizontal box dimension being comparable to the depth and the other much larger. In particular, we shall take $a_2 = 1{\cdot}0$, so that only x-rolls are predicted by linear theory. It is the interaction of rolls that we shall address. Although we must develop the theory for Rayleigh number $R \neq 0$ for completeness properties of the differential system, we shall, with no loss of generality, set $R = 0$ at the end. Hence, pure Marangoni instability will be analysed.

Let us restate the linear stability problem for the case at hand:

$$\nabla^2\mathbf{v} - \nabla p + M^{-1}R\theta\hat{\mathbf{z}} = \mathbf{0}, \tag{4.1a}$$

$$\nabla . \mathbf{v} = 0, \tag{4.1b}$$

$$\nabla^2\theta + Mw = 0, \tag{4.1c}$$

with

$$\theta = u = w = 0 \qquad (z = 0), \tag{4.1d}$$

$$\theta_z = w = u_z + \theta_x = 0 \quad (z = 1), \tag{4.1e}$$

$$\theta_x = u = w_x = 0 \quad (x = 0, a_1). \tag{4.1f}$$

The problem is now a two-dimensional problem, since we are interacting only x-rolls; hence v, $\partial/\partial y \equiv 0$.

For fixed $\hat{M}$ the eigenvalues are denoted by R_{mj}, with $m, j = 1, 2, \ldots$, and m is the horizontal wavenumber while j is the vertical wavenumber. Define

$$\lambda_m = m\pi/a_1. \tag{4.2}$$

The eigenfunctions are

$$u_{mj} = -\lambda_m^{-1}\sin\lambda_m x\, DY_{mj}(z), \tag{4.3a}$$

$$w_{mj} = \cos\lambda_m x\, Y_{mj}(z), \tag{4.3b}$$

$$\theta_{mj} = \cos\lambda_m x\, X_{mj}(z), \tag{4.3c}$$

where the X_{mj} and Y_{mj} are the eigensolutions of the system (A 1)–(A 4) of part 1.

The adjoint problem is

$$\nabla^2\mathbf{v}^* - \nabla p^* + \hat{M}\theta\hat{\mathbf{z}} = \mathbf{0}, \tag{4.4a}$$

$$\nabla . \mathbf{v}^* = 0, \tag{4.4b}$$

$$\nabla^2\theta^* + \hat{M}^{-1}Rw^* = 0, \tag{4.4c}$$

with

$$\theta^* = u^* = w^* = 0 \qquad (z = 0), \tag{4.4d}$$

$$\theta^*_z + w^*_z = w^* = u^*_z = 0 \quad (z = 1), \tag{4.4e}$$

$$u^* = w^*_x = \theta^*_x = 0 \qquad (x = 0, a_1). \tag{4.4f}$$

The adjoint eigenfunctions are

$$u^*_{mj} = -\lambda_m \sin\lambda_m x\, DY^*_{mj}(z), \tag{4.5a}$$

$$w^*_{mj} = \lambda^2_m \cos\lambda_m x\; Y^*_{mj}(z), \tag{4.5b}$$

$$\theta^*_{mj} = \cos\lambda_m x\, X^*_{mj}(z), \tag{4.5c}$$

where X^*, Y^* satisfy the system (A 5)–(A 8) of part 1.

It is worth mentioning a slight difference in the analysis between part 1 and the present paper. Here the case (0, 0) does *not* correspond to an allowable mode, but contributes to the mean temperature. Hence we first must subtract the mean before using the eigenfunction expansion. In part 1 the mode $m = 0$ was allowable, and all the modes $m \neq 0$ as well as $m = 0$ contributed to the mean. Hence it was not necessary to subtract the mean first, and direct application of the eigenfunction expansion was made.

We now decompose all dependent variables into horizontal mean (i.e. x-mean) plus departures from the mean as follows:

$$\mathbf{v} = \bar{\mathbf{v}} + v', \quad \theta = \bar{\theta} + \theta', \quad p = \bar{p} + p', \tag{4.6a}$$

where, for each quantity g,

$$\bar{g} = \frac{1}{a_1}\int_0^{a_1} g\,dx. \tag{4.6b}$$

For the case $R = 0$, the equations (2.1)–(2.3) are

$$\nabla^2\mathbf{v} - \nabla p = MPr^{-1}\{\mathbf{v}_t + (\mathbf{v}.\nabla)\,\mathbf{v}\}, \tag{4.7a}$$

$$\nabla.\mathbf{v} = 0, \tag{4.7b}$$

$$\nabla^2\theta + Mw = M\{\theta_t + (\mathbf{v}.\nabla)\,\theta\}. \tag{4.7c}$$

If the forms (4.6) are introduced into system (4.7), we get

$$\nabla^2\bar{\mathbf{v}} - \nabla\bar{p} = MPr^{-1}\{\bar{\mathbf{v}}_t + (\bar{\mathbf{v}}.\nabla)\bar{\mathbf{v}} + \overline{(\mathbf{v}'.\nabla)\,\mathbf{v}'}\}, \tag{4.8a}$$

$$\nabla.\bar{\mathbf{v}} = 0, \tag{4.8b}$$

$$\nabla^2\bar{\theta} + M\bar{w} = M\{\bar{\theta}_t + (\bar{\mathbf{v}}.\nabla)\,\bar{\theta} + \overline{(\mathbf{v}'.\nabla)\,\theta'}\}, \tag{4.8c}$$

and

$$\nabla^2\mathbf{v}' - \nabla p' = MPr^{-1}\{\mathbf{v}'_t + (\mathbf{v}'.\nabla)\,\bar{\mathbf{v}} + (\bar{\mathbf{v}}.\nabla)\,\mathbf{v}' + [(\mathbf{v}'.\nabla)\,\mathbf{v}']_f\}, \tag{4.9a}$$

$$\nabla.\mathbf{v}' = 0, \tag{4.9b}$$

$$\nabla^2\theta' + Mw' = M\{\theta'_t + (\mathbf{v}'.\nabla)\,\bar{\theta} + (\bar{\mathbf{v}}.\nabla)\,\theta' + [(\mathbf{v}'.\nabla)\,\theta']_f\}, \tag{4.9c}$$

where $[\ ]_f$ denotes the fluctuating part of [ ]. The same boundary conditions hold for both systems (4.8) and (4.9).

As is well-known, there is no mean velocity field induced by the convection, and thus

$$\bar{\mathbf{v}} = \mathbf{0}. \tag{4.10a}$$

Equation (4.8c) then simplifies considerably, and for steady or quasi-static convection,

$$\bar{\theta}_z = M\overline{(w'\theta')}. \tag{4.10b}$$

If these relations are used to simplify (4.7), we obtain

$$\nabla^2\mathbf{v}' - \nabla p' = MPr^{-1}\{\mathbf{v}'_t + [(\mathbf{v}'.\nabla)\mathbf{v}']_f\}, \tag{4.11a}$$

$$\nabla.\mathbf{v}' = 0, \tag{4.11b}$$

$$\nabla^2\theta' + Mw' = M\{\theta'_t + Mw'\overline{(w'\theta')} + [(\mathbf{v}'.\nabla)\theta']_f\}. \tag{4.11c}$$

We now take the scalar product of (4.11 a, c) with the adjoint vectors $(\mathbf{v}^*_{mj}, \theta^*_{mj})$ at $M = M_c$, $R = R_{mj}$, and integrate over the fluid volume. This gives

$$(M - M_c)\langle\theta^*_{mj}w'\rangle - M_c^{-1}R^*_{mj}\langle w^*_{mj}\theta'\rangle = M\langle\theta^*_{mj}\theta'_t + Pr^{-1}\mathbf{v}^*_{mj}.\mathbf{v}'_t\rangle$$
$$+ M\langle\theta^*_{mj}\{[(\mathbf{v}'.\nabla)\theta']_f + Mw'\overline{(w'\theta')}\} + Pr^{-1}\mathbf{v}^*_{mj}.[(\mathbf{v}'.\nabla)\mathbf{v}']_f\rangle \tag{4.12}$$

for each m and j. Equation (4.12) is the basis for the derivation of the amplitude equations, and is analogous to equation (5.19) of part 1.

5. Simple and double interactions

5.1. *Simple eigenvalue for* (1, 0)

Let us consider an aspect ratio $a_1 = 1{\cdot}5$, which corresponds in figure 2 to a simple eigenvalue M_c for convection with $(m_1, m_2) = (1, 0)$.

We find that

$$M_c = 79{\cdot}4, \tag{5.1}$$

and by hypothesis $R_{11} = 0$. The quadratic interaction of mode 11 generates the 21 mode $(R_{21} \neq 0)$ so the set $\mathscr{S}$ is

$$\mathscr{S} = \{11, 21\}. \tag{5.2a}$$

We write

$$(\theta', \mathbf{v}') = A_1(\theta_{11}, \mathbf{v}_{11}) + A_2(\theta_{21}, \mathbf{v}_{21}), \tag{5.2b}$$

and substitute into (4.12). We obtain

$$\nu_1\dot{A}_1 = (M - M_c)A_1 - Z_1, \tag{5.3a}$$

$$\nu_2\dot{A}_2 = -M_c^{-1}R_2 f_2 A_2 - Z_2, \tag{5.3b}$$

when $M = M_c$, where

$$\nu_m = d_m^{-1}M_c\langle\theta^*_{m1}\theta_{m1} + Pr^{-1}\mathbf{v}^*_{m1}.\mathbf{v}_{m1}\rangle, \tag{5.3c}$$

$$f_m = d_m^{-1}\langle w^*_{m1}\theta_{m1}\rangle, \tag{5.3d}$$

$$d_m = \langle\theta^*_{m1}w_{m1}\rangle. \tag{5.3e}$$

We shall not give all the details of the evaluations, since they are parallel to those of part 1. After a good deal of algebraic manipulation, we find that, if α_1, α_2 and β_1 are constants,

$$Z_1 = \alpha_1 A_1 A_2 + \beta_1 A_1^3, \tag{5.3f}$$

$$Z_2 = \alpha_2 A_1^2, \tag{5.3g}$$

Pr	$\nu_1 \times 10^{-4}$	$\omega_1 \times 10^{-4}$
0·1	0·37	5·2
1·0	0·13	0·64
10·0	0·10	0·43
∞	0·10	0·41

TABLE 1

and the governing amplitude equation takes the form

$$\nu_1 \dot{A}_1 = (M - M_c) A_1 - \omega_1 A_1^3. \tag{5.4}$$

The computations of the coefficients have been performed for various values of Prandtl number, and some results are shown in Table 1. Since $\omega_1 > 0$, the convective state results from supercritical bifurcation and is stable.

5.2. *Simple eigenvalue for* (2, 0)

Let us consider an aspect ratio $a_1 = 3.1$, which corresponds in figure 2 to a simple eigenvalue M_c for convection with $(m_1, m_2) = (2, 0)$. We find that

$$M_c = 79{\cdot}2. \tag{5.5}$$

There is again a quadratic interaction and the set $\mathscr{S}$ is

$$\mathscr{S} = \{21, 41\}. \tag{5.6}$$

We omit all details and state the final amplitude equation

$$\nu_2 \dot{A}_2 = (M - M_c) A_2 - \omega_2 A_2^3, \tag{5.7}$$

where the coefficients have the numerical values given in table 2. Again, $\omega_2 > 0$, the convective state results from supercritical bifurcation and is stable.

5.3. *Double eigenvalues for* (1, 0) *and* (2, 0)

Let us consider an aspect ratio $a_1 = 2{\cdot}21$, which corresponds in figure 2 to a double eigenvalue for convection with $(m_1, m_2) = (1, 0)$ and $(m_1, m_2) = (2, 0)$. We find that

$$M_c = 90{\cdot}2. \tag{5.8}$$

The quadratic interaction of modes 11 and 21 generates modes 31 and 41. The set $\mathscr{S}$ is

$$\mathscr{S} = \{11, 21, 31, 41\}. \tag{5.9a}$$

We write

$$(\theta', \mathbf{v}') = \sum_{i=1}^{4} A_i(\theta_{i1}, \mathbf{v}_{i1}), \tag{5.9b}$$

and substitute into (4.12). We obtain

$$\nu_1 \dot{A}_1 = (M - M_c) A_1 - Z_1, \tag{5.10a}$$

$$\nu_2 \dot{A}_2 = (M - M_c) A_2 - Z_2, \tag{5.10b}$$

$$M_c^{-1} R_3 f_3 A_3 = -Z_3, \tag{5.10c}$$

$$M_c^{-1} R_4 f_4 A_4 = -Z_4, \tag{5.10d}$$

Pr	$\nu_2 \times 10^{-4}$	$\omega_2 \times 10^{-3}$
0·1	0·44	1·4
1·0	0·13	0·26
10·0	0·10	0·25
∞	0·098	0·25

TABLE 2

Pr	$\nu_1 \times 10^{-4}$	$\nu_2 \times 10^{-3}$	$\alpha_1 \times 10^{-3}$	$\alpha_2 \times 10^{-2}$	$\beta_1 \times 10^{-3}$	$\sigma_1 \times 10^{-4}$	$\sigma_2 \times 10^{-4}$	$\omega_2 \times 10^{-3}$
0·1	0·58	3·9	−0·88	1·5	0·18	2·3	1·3	5·0
1·0	0·23	1·2	−0·34	0·43	0·18	0·33	0·17	0·95
10·0	0·20	0·90	−0·29	0·32	0·18	0·24	0·12	0·77
∞	0·20	0·87	−0·29	0·31	0·18	0·23	0·12	0·76

TABLE 3

when $M = M_c$. Here the f_3, f_4, R_3, R_4 and functionals Z_1–Z_4 are defined in analogous way to those in part 1. Again we omit details, and state the final amplitude equations:

$$\nu_1 \dot{A}_1 = (M-M_c)A_1 - \alpha_1 A_1 A_2 - \beta_1 A_1^3 - \sigma_1 A_1 A_2^2, \tag{5.11a}$$

$$\nu_2 \dot{A}_2 = (M-M_c)A_2 - \alpha_2 A_1^2 - \sigma_2 A_1^2 A_2 - \omega_2 A_2^3. \tag{5.11b}$$

Numerical values of the coefficients are given in table 3. We analyse the equations (5.11) in detail below.

5.4. *Double eigenvalue for* (2, 0) *and* (3, 0)

Let us consider an aspect ratio $a_1 = 3{\cdot}81$, which corresponds in figure 2 to a double eigenvalue for convection with $(m_1, m_2) = (2, 0)$ and $(m_1, m_2) = (3, 0)$. We find that

$$M_c = 82{\cdot}9. \tag{5.12}$$

The quadratic interaction of modes 21 and 31 generates modes 11, 41, 51, 61, so the set $\mathscr{S}$ is

$$\mathscr{S} = \{11, 21, 31, 41, 51, 61\}. \tag{5.13a}$$

We write

$$(\theta', \mathbf{v}') = \sum_{i=1}^{6} A_i(\theta_{i1}, \mathbf{v}_{i1}), \tag{5.13b}$$

and substitute into (4.2). We obtain

$$\nu_2 \dot{A}_2 = (M-M_c) - Z_2, \tag{5.14a}$$

$$\nu_3 \dot{A}_3 = (M-M_c) - Z_3, \tag{5.14b}$$

$$M_c^{-1} R_n f_n A_n = -Z_n \quad (n = 1, 4, 5, 6), \tag{5.14c}$$

when $M = M_c$. Here the f_n, R_n, Z_n are defined in an analogous way to those in part 1. Rather than give the details, we state the final amplitude equations:

$$\nu_2 \dot{A}_2 = (M-M_c)A_2 - \omega_2 A_2^3 - \tau_2 A_2 A_3^2, \tag{5.15a}$$

$$\nu_3 \dot{A}_3 = (M-M_c)A_3 - \tau_3 A_2^2 A_3 - \omega_3 A_3^3, \tag{5.15b}$$

and the coefficients are given in table 4.

Pr	$\nu_2 \times 10^{-4}$	$\nu_3 \times 10^{-3}$	$\omega_2 \times 10^{-4}$	$\tau_2 \times 10^{-3}$	$\omega_3 \times 10^{-3}$	$\tau_3 \times 10^{-3}$
0·1	0·46	3·6	1·4	−7·8	5·1	6·7
1·0	0·18	1·2	0·17	−1·1	0·85	1·2
10·0	0·15	0·92	0·12	−0·76	0·66	0·89
∞	0·14	0·89	0·11	−0·72	0·64	0·86

TABLE 4

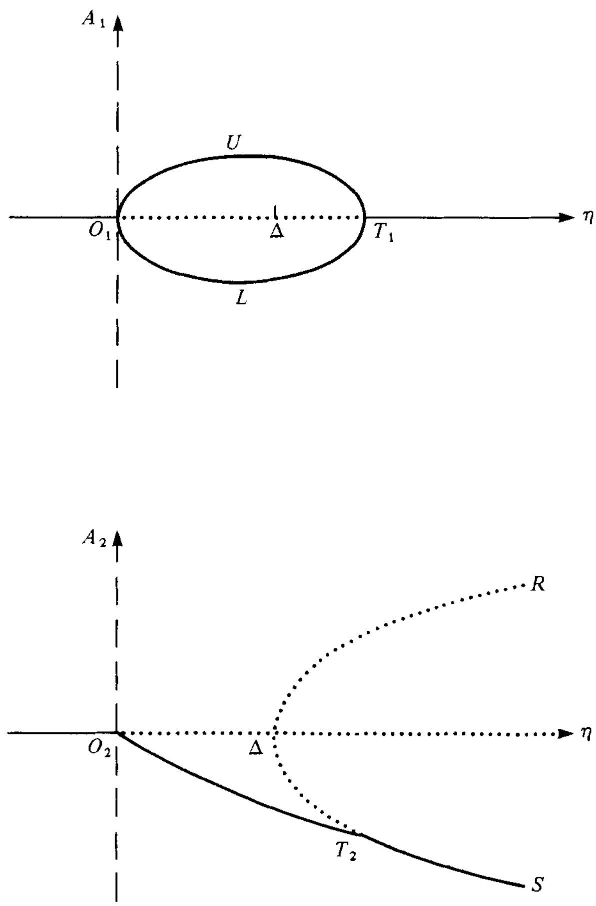

FIGURE 8. The bifurcation diagram for $a_2 = 1{\cdot}5$, and a_1 slightly less than 3·1, wnere $\Delta = M_2 - M_1$. Solid lines represent stable branches while dotted lines represent unstable branches.

6. Analysis and discussion

In the cases of §§5.1 and 5.2, the self-interaction of roll cells (1, 0) and (2, 0) is considered. In both cases, the interaction is governed by single amplitude equations containing cubic but no quadratic nonlinearities. These are (5.4) and (5.7) respectively. The values ν_1 and ν_2, depending on Prandtl number Pr, are values from the linear stability problem, and for given λ of (3.3) are identical here with those of part 1. Careful comparison shows this. The values ω_1 and ω_2 of (5.4) and (5.7) are always positive, so that these simple self-interactions always correspond to stable supercritical

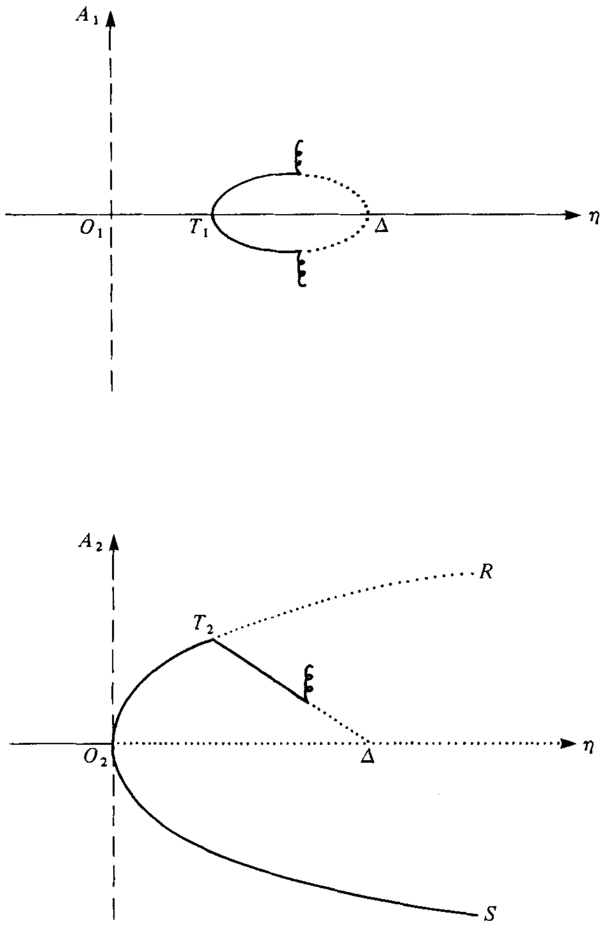

FIGURE 9. The bifurcation diagrams for $a_2 = 1{\cdot}5$, and a_1 slightly greater than $3{\cdot}1$, where $\Delta = M_1 - M_2$. Solid lines represent stable branches while dotted lines represent unstable branches. The curly lines represent time-periodic bifurcations. The orientations of these branches and their stability properties are unknown.

bifurcation. It is easy to show that for *any* values $(m_1, m_2) \neq (0,0)$ indicated in figure 7 self-interactions always have amplitude equations of the same form, i.e.

$$\nu \dot{A} = (M - M_c)\,A - \omega A^3, \tag{6.1}$$

where $\nu > 0$. Presumably, $\omega > 0$ for any of these, so that stable, supercritical bifurcation is always predicted for self-interactions. This is likewise true in the case of the circular container of part 1 for $m \neq 0$. It is only for the $(m = 0)$ axisymmetric mode that (6.1) is augmented by a quadratic term. Thus the axisymmetric mode bifurcates subcritically, and so has snap-through and hysteresis properties as discussed in part 1.

In the case of § 5.3 the interaction of modes (1, 0) and (2, 0) is examined near the double eigenvalue at $a_1 = 3{\cdot}1$ of figure 2. The governing amplitude equations (5.11) are a pair of coupled equations identical in form with equations (7.10) and (7.11) of part 1, which govern the interaction of modes $m = 1$ and $m = 2$ near their double eigenvalue. Again, the ν_i are linear-theory values that depend on Pr and λ, but not on

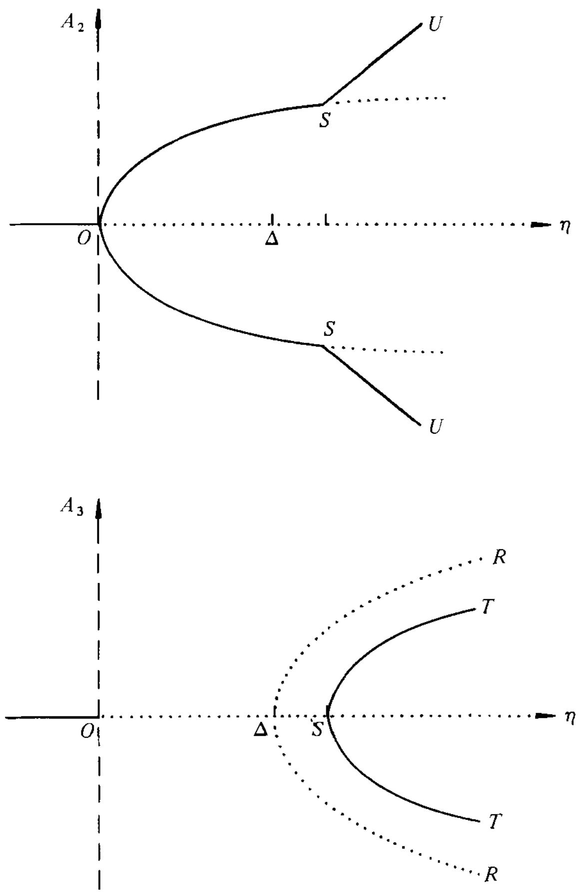

FIGURE 10. The bifurcation diagrams for $a_2 = 1{\cdot}5$, and a_1 slightly less than $3{\cdot}81$, where $\Delta = M_3 - M_2$. Solid lines represent stable branches while dotted lines represent unstable branches.

the cylinder geometry. Although the coefficients are not identical in the two cases, all of the qualitative predictions are. Figure 8 shows the results of our analysis of (7.10)–(7.11) for $a_1 < 3{\cdot}1$. The mixed mode containing both modes (1, 0) and (2, 0) bifurcates supercritically at M_c, and, as M is further increased, A_1 follows either $O_1\,UT_1$ or $O_2\,LT_1$, while A_2 follows $O_2\,T_2$. At a value of $\eta \equiv M - M_1$ greater than $\Delta \equiv M_2 - M_1$, there is secondary bifurcation to a pure mode $m = 2$. This branch is labelled T_2S.

Figure 9 shows the situation for $a_1 > 3{\cdot}1$. Here, as M crosses M_c, the pure mode $m = 2$ bifurcates supercritically and follows either curve $O_2\,T_2$ or $O_2\,S$. However, for $\eta \equiv M - M_2$ less than $\Delta \equiv M_1 - M_2$, the pure mode persists but only on the branch $O_2\,S$. Again, there is the possibility of branch $O_2\,T_2$ bifurcating first to the mixed mode and then to time-periodic convection. The amplitude equations (5.11) are in form identical with those governing hexagonal cells as predicted by Scanlon & Segel (1967) for horizontally unbounded layers. However, since the contexts are quite different, the coefficients are quite different. Scanlon & Segel find subcritical hexagons. We find only supercritical convection of mixed mode or pure mode $m = 2$.

In the case of § 5.4, the interaction of modes (2, 0) and (3, 0) is examined near the double eigenvalue at $a_1 = 3{\cdot}81$ of figure 2. The governing amplitude equations (5.15)

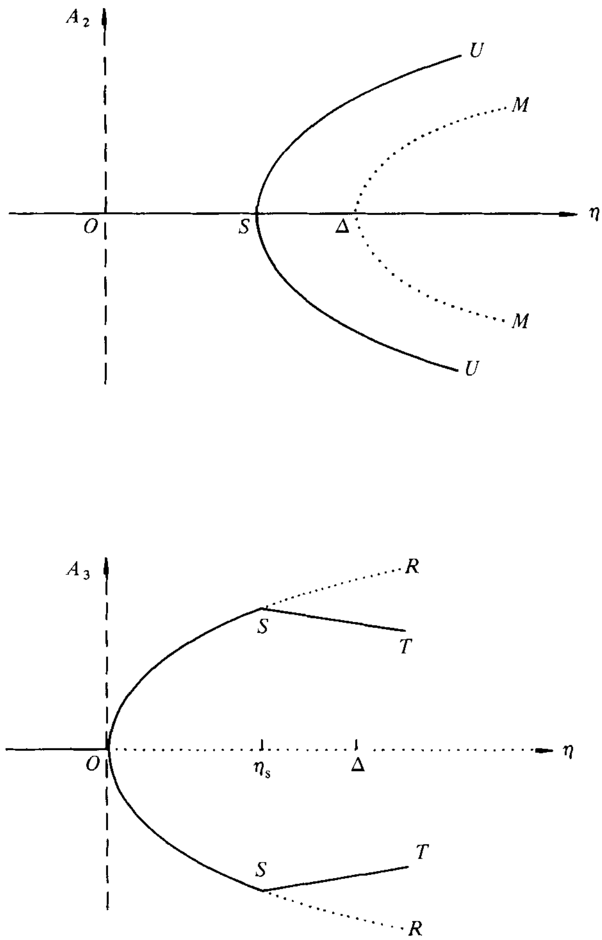

FIGURE 11. The bifurcation diagrams for $a_2 = 1{\cdot}5$, and a_1 slightly greater than 3·81 where $\Delta = M_2 - M_3$. Solid lines represent stable branches while dotted lines represent unstable branches.

are a pair of coupled equations. Again, ν_i are linear-theory values that depend on *Pr* and λ, but not on the cylinder geometry. Figure 10 shows the situation for $a_1 < 3{\cdot}81$. The pure mode $(2, 0)$ bifurcates supercritically at M_c, $\eta \equiv M - M_2 = 0$, and steady convection follows either branch OS as M increases. At a value of $\eta > \Delta \equiv M_2 - M_1$ there is secondary bifurcation to the mixed mode containing both modes $(2, 0)$ and $(3, 0)$, and, as M increases further, A_2 follows either branch SU and A_3 follows a branch ST. Figure 11 shows the situation for $a_1 > 3{\cdot}81$. Here, at M_c, the pure mode $(3, 0)$ bifurcates supercritically and follows either branch OS until

$$\eta \equiv M - M_3 = \eta_s < \Delta \equiv M_2 - M_3.$$

Here there is secondary bifurcation to a mixed mode in which A_2 follows either SU, and A_2 follows an ST. The sequence of events here, near $a = 3{\cdot}81$, has no counterpart in part 1, since there was no double eigenvalue there for modes $m = 2$ and $m = 3$. However, the amplitude equations (5.15) have the form typical of Rayleigh–Bénard convection in containers, as discussed by Rosenblat (1982). Figures 10 and 11 are qualitatively similar to Rosenblat's results, which apply to the buoyancy-driven convection.

In summary, we again find that interactions near double eigenvalues give qualitative features that strongly distinguish behaviour for aspect ratios on one side from behaviour on the other side. Parallels as well as differences in behaviour exist between the circular and rectangular cases.

This work was supported by NASA–Lewis Research Center through Contract no. NAS3-22274.

REFERENCES

Beck, J. L. 1972 *Phys. Fluids* **15**, 1377.

Davis, S. H. 1967 *J. Fluid Mech.* **30**, 465.

Pearson, J. R. A. 1958 *J. Fluid Mech.* **4**, 489.

Rosenblat, S. 1979 *Stud. Appl. Math.* **60**, 241.

Rosenblat, S. 1982 Pending publication.

Rosenblat, S., Davis, S. H. & Homsy, G. M. 1982 *J. Fluid Mech.* **120**, 91.

Scanlon, J. W. & Segel, L. A. 1967 *J. Fluid Mech.* **30**, 149.